

# Influence of the definition of dissipative events on their statistics

E. Buchlin<sup>1,2</sup>, S. Galtier<sup>1</sup>, and M. Velli<sup>2,3</sup>

<sup>1</sup> Institut d’Astrophysique Spatiale, CNRS – Université Paris-Sud, Bât. 121, 91405 Orsay Cedex, France

<sup>2</sup> Dipartimento di Astronomia e Scienza dello Spazio, Università di Firenze, 50125 Firenze, Italy

<sup>3</sup> Istituto Nazionale Fisica della Materia, Sezione A, Università di Pisa, 56100 Pisa, Italy

Received : / Revised date :

**Abstract** A convenient and widely used way to study the turbulent plasma in the solar corona is to do statistics of properties of events (or structures), associated with flares, that can be found in observations or in numerical simulations. Numerous papers have followed such a methodology, using different definitions of an event, but the reasons behind the choice of a particular definition (and not another one) is very rarely discussed. We give here a comprehensive set of possible event definitions starting from a one-dimensional data set such as a time-series of energy dissipation. Each definition is then applied to a time-series of energy dissipation issued from simulations of a shell-model of magnetohydrodynamic turbulence as defined in Giuliani and Carbone (1998), or from a new model of coupled shell-models designed to represent a magnetic loop in the solar corona. We obtain distributions of the peak dissipation power, total energy, duration and waiting-time associated to each definition. These distributions are then investigated and compared, and the influence of the definition of an event on statistics is discussed. In particular, power-law distributions are more likely to appear when using a threshold. The sensitivity of the distributions to the definition of an event seems also to be weaker for events found in a highly intermittent time series. Some implications on statistical results obtained from observations are discussed.

**Key words.** Sun: corona, flares – MHD – Methods: data analysis

## 1. Introduction

The mechanism heating the solar corona to millions of degrees remains an open problem, but it is generally understood that a great part of the energy dissipation must occur at scales that are smaller than the structures that can be resolved by observations ( $\approx 100$  km), as small as 10–100 m (the Kolmogorov turbulent cascade dissipation scale). One of the most successful approaches to reach this four-order-of-magnitude wide gap is to assume that the statistics obtained at observable scales are still valid at smallest scales. The properties of the global system, from observable to non-observable scales, can then be investigated. This is for example the idea underlying Hudson’s (1991) critical power-law slope of  $-2$  for the distribution of flare energies.

The measurement of the power-law slope for the lowest energy flares has indeed been a major goal of coronal physics in the last decade. Aschwanden *et al.* (2000) has summarized the distributions of event energies that were obtained at wavelengths from X-rays to ultra-violet (UV), and for event energies covering a range of eight orders of magnitude from  $10^{17}$  J (“nanoflares”) to  $10^{25}$  J (“flares”). It seems — and it is a statement of Aschwanden *et al.* (2000) — that these distributions can be matched together to form a unique power-law distribution of slope  $\approx -1.8$ .

However, for the smallest events, mainly observed in UV by filter imaging instruments, some observations seem not to mutually agree, and they seem not to fit in the global distribution. A possible explanation for this is given by Aschwanden and Charbonneau (2002): the energy of an event could be wrongly deduced from the observable quantities (like intensity in some spectral lines), leading to a systematic error in the distribution of event energies. Another explanation could be that all authors do not agree on what they mean by “event”, *i.e.* the fact that inequivalent definitions exist in the literature.

Indeed, defining an event is likely to be much more difficult for low energy events than for high energy events. For high-energy events, whose distributions are in general derived from X-rays and radio observations, there is little ambiguity on what is an event: events are very rare ( $10^{-6}$  s $^{-1}$  for the whole solar disk between  $10^{23}$  and  $10^{24}$  J) and well-separated by long low-flux times. On the contrary, low-energy events can be very close in space and time, making it difficult to separate them, either because they occur on the same line-of-sight or because they are smaller than the instrumental resolution or shorter than the time resolution. The difficulty is even bigger if we subscribe to the idea that the corona is in a self-organized critical state so that small events trigger other events, leading to avalanches as illustrated by the sandpile paradigm (Bak *et al.*, 1988; Lu and Hamilton, 1991): among all these events, which ones should be used to do statistics?

We think that this difficulty has been underestimated when statistics obtained from observations or simulations by different methods have been compared. In fact, the definition of an event which is used is very rarely discussed (contrary to the influence of the relationship between the observable parameters and the physical variables of an event), and is sometimes even not given precisely.

In this paper we give some definitions that could be used, mainly inspired from definitions which have already been used in the past. We choose to restrain ourselves to events defined from a one-dimensional data set, namely a time series of energy dissipation, so that the definitions can be easily compared. We then produce statistics of events (histograms of event energies, durations and waiting times), for different definitions of an event, and compare them. The time series we use are the data output by a shell-model of MHD turbulence (Giuliani and Carbone, 1998), and by a new model of coupled shell-models describing Alfvén turbulence in a coronal loop (Buchlin *et al.*, 2004). However, the aim of this paper is not to study shell-models of MHD, but to see to which extent the definition of events influences their statistics, even in a simple case of events detected in a time series of energy dissipation.

## 2. Event definitions

We present here a basic list of possible definitions of an event when a “signal”  $\epsilon(t)$ , which is the time series of the power dissipated in the system, is given (Fig. 1). Most of the ideas of this list come from the definitions that have been chosen in papers found in the literature. For each event, we get:

- $E$ , the total energy dissipated during the event,
- $P$ , the peak power of energy dissipation,
- $T$ , the duration of the event,
- $t_e$ , the time of the event, necessary to obtain the waiting times  $\tau_w$ , *i.e.* the (quiescent) time between two consecutive events.

### 2.1. Peaks

**Definition 1 (peak).** An event corresponds to a local maximum  $\epsilon(t_m)$  in the signal  $\epsilon(t)$ . The time of the event is  $t_e = t_m$ , the peak dissipation power is  $P = \epsilon(t_e)$ , the total dissipated energy is  $E = \int_{t_a}^{t_b} \epsilon(t) dt$  where  $t_a$  and  $t_b$  are the two local minima around  $t_e$ , and the event duration is  $T = t_b - t_a$ .

**Variant 1.1 (peak-background).** The background  $b(t)$  is the affine function defined between the points  $(t_a, \epsilon(t_a))$  and  $(t_b, \epsilon(t_b))$ . With the notations of definition 1, the time of the event is  $t_e$ , the peak dissipation power is  $P - b(t_e)$ , the total dissipated energy is  $E - \int_{t_a}^{t_b} b(t) dt = E - (\epsilon(t_a) + \epsilon(t_b)) \cdot T/2$ , and the event duration is  $T$ .

### 2.2. Threshold

**Definition 2 (threshold).** A threshold  $\epsilon_{\text{thr}}$  is chosen, and an event is a part of the signal  $\epsilon(t)$  which stays above  $\epsilon_{\text{thr}}$ : more precisely, it is a maximal connex part  $V = [t_a, t_b]$  of the set

$\{t \mid \epsilon(t) > \epsilon_{\text{thr}}\}$ . The total dissipated energy is  $E = \int_V \epsilon(t) dt$ , the peak dissipation power is  $P = \max_V \epsilon(t)$  and the event duration is  $T = t_b - t_a$ . The time of the event is the time at which the maximum of  $\epsilon(t)$  on  $V$  is attained:  $\epsilon(t_e) = \max_V \epsilon(t)$ .

There are several other alternatives to define the time of the event, like  $t_e = (t_b + t_a)/2$  (the middle of interval  $V$ ) or  $t_e = \frac{1}{E} \int_V \epsilon(t) \cdot t dt$  (the barycenter of the event, weighted by  $\epsilon$ ). But these variants do not change the statistics of  $P$ ,  $E$ , and  $T$ , and they seem to have little influence on the statistics of  $\tau_w$ .

We can consider the threshold level  $\epsilon_{\text{thr}}$  as a background level, giving the following definition:

**Variant 2.1 (threshold-background).** Using definition 2 and its notations, the time of the event is  $t_e$ , the peak dissipation power is  $P - \epsilon_{\text{thr}}$ , the total dissipated energy is  $E - \int_V \epsilon_{\text{thr}} dt = E - \epsilon_{\text{thr}} \cdot T$ , and the event duration is  $T$ .

The threshold can be chosen as a function of the overall average  $\bar{\epsilon}$  and standard deviation  $\sigma_\epsilon$  of  $\epsilon(t)$ . It can also be chosen iteratively, by using the average and standard deviation of the time series during the quiescent times between events (which have been defined by the previous iteration of this process), as in Boffetta *et al.* (1999).

### 2.3. Wavelet analysis

This method assumes that we have built the time-scale plane  $y(t_0, s)$  for  $\epsilon(t)$ , by convolution of  $\epsilon(t)$  by the wavelets  $w_{t_0, s}(t) = 1/s \cdot w_0((t - t_0)/s)$ . A mother wavelet  $w_0$  which seems well adapted to the shape of events is the second derivative of a Gaussian (“Mexican hat”). When the noise is in  $1/f$ , Sanz *et al.* (2001) have shown that the Mexican hat is the best wavelet to find enhancements of the signal.

**Definition 3 (wavelet).** An event corresponds to a local maximum  $y(t_e, s_e)$  in the time-scale plane  $y(t_0, s)$ . The time of the event is  $t_e$ , its duration  $T$  is the scale  $s_e$ , its total energy is  $E = y(t_e, s_e)$ . Its peak power  $P$  can be defined as  $\max_V \epsilon(t)$  with  $V = [t_e - s_e/2, t_e + s_e/2]$ .

For better accuracy in the definition of  $s_e$  and  $t_e$ , we need to have a good resolution in the time-frequency plane, *i.e.* we use a continuous wavelet transform. As a result, and also because we have used the Mexican hat wavelet, the wavelets are non-orthogonal, and there is a risk to find several non-independent events where there is only one event. To avoid this, it is possible to impose that two events are separated by at least some distance in the time-scale plane (typically a factor 2 in scale and an interval  $s_e$  in time), but in practice this is not necessary as the time-scale plane is sufficiently smooth.

## 3. Model time series

### 3.1. Shell-model

The results of the next section are based on data output from a shell-model of incompressible MHD turbulence. In such models (Gloaguen *et al.*, 1985; Biskamp, 1994; Frick and Sokoloff,

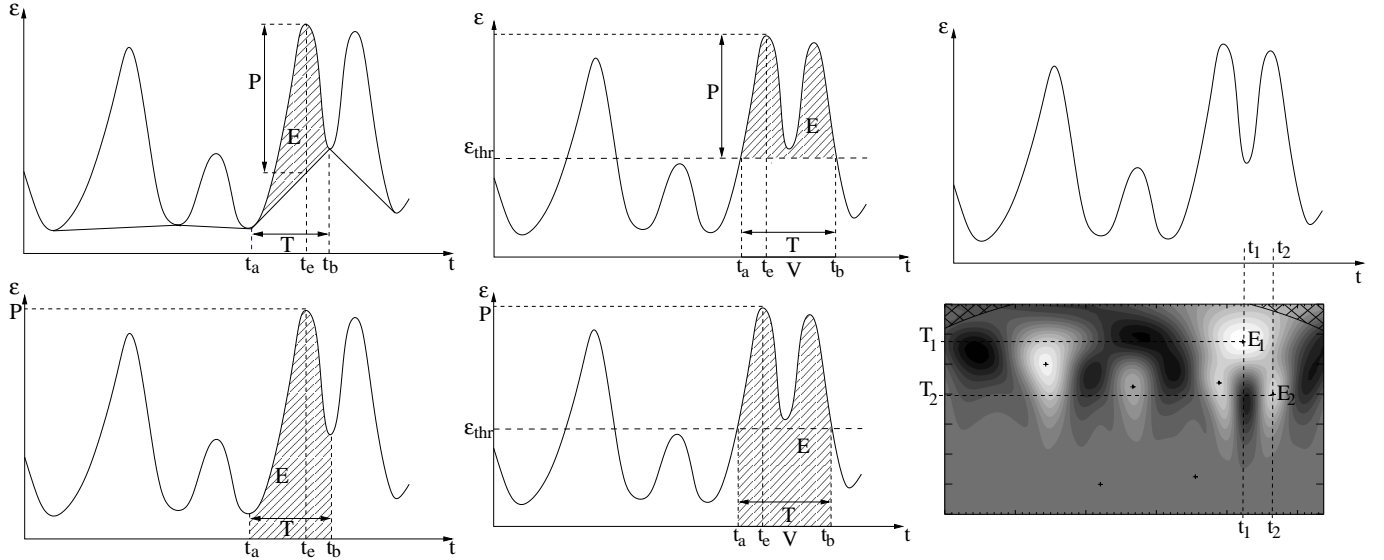


Figure 1: Definitions of events and of event characteristics ( $t_e$ ,  $T$ ,  $P$ , and  $E$ ). Left: peaks (definition 1), with (top) and without (bottom) background detection. Middle: threshold (definition 2), with (top) or without (bottom) taking the background into account. Right: peaks in the wavelets time-frequency plane (definition 3). For this definition, events are marked as crosses in the time-frequency plane, indicating the event time  $t_e$  and duration  $T$ . The total energy  $E$  is the wavelet amplitude (color) at this position.

1998; Giuliani and Carbone, 1998), the Fourier wavenumber space is divided in concentric shells  $S_n = \{\mathbf{k} \mid \|\mathbf{k}\| \in [k_n, k_{n+1}]\}$  with  $k_n = k_0 \lambda^n$  and usually  $\lambda = 2$ . A single complex scalar value  $u_n$  represents the velocity increments  $|u(x + \ell) - u(x)|$  on scales  $\ell$  for  $2\pi/\ell \in S_n$ . The same holds for the scalar value  $b_n$  representing the magnetic field increments on the same scales  $\ell$ . This model is the magnetohydrodynamic analog of the GOY (Gledzer-Ohkitani-Yamada: Gledzer, 1973; Yamada and Ohkitani, 1987, 1988a,b) shell-model of fluid turbulence. It is governed by the following equations, given in Giuliani and Carbone (1998):

$$\frac{dZ_n^s}{dt} = -k_n^2(\nu^+ Z_n^s + \nu^- Z_n^{-s}) + ik_n T_n^{s*} + f_n^s \quad (1)$$

where  $Z_n^s = v_n + sb_n$  are the Elsässer variables,  $s = \pm$ ,  $\nu^s = (\nu + s\eta)/2$  are combinations of kinematic viscosity and resistivity,  $f_n^s$  are external driving forces, and  $T_n^s$  is the term corresponding to local non-linear interactions between shells. For a given shell  $n$ , this term involves the neighbors and second-nearest neighbors of the shell  $n$ , modelling local interactions between triads of consecutive modes. The detailed coefficients of this term are given in Giuliani and Carbone (1998) and depend on the dimensionality (e.g. 2D or 3D) of the physical MHD system the shell-model represents, via the conservation of the MHD invariants.

This model can describe the evolution of modes over a wide range of wavenumbers with just a few dozens of degrees of freedom. It is thus very interesting for studying MHD turbulence with high Reynolds numbers, and intermittency. It actually exhibits typical properties of MHD turbulence, from wide power-law spectra to dynamo effect in 3D (Giuliani and Carbone, 1998), including spatial and tempo-

ral intermittency (Giuliani and Carbone, 1998; Boffetta *et al.*, 2002).

The equations 1 are solved numerically and we get the time series of dissipated power  $\epsilon(t) = \sum_n k_n^2(\nu|u_n(t)|^2 + \eta|b_n(t)|^2)$ , which is our variable of interest. To obtain the first time series shown on Fig. 2, hereafter known as the time series  $\langle 1 \rangle$ , we used 24 shells (representing  $k = 1$  to  $k \approx 8.4 \cdot 10^6$ ), with  $\lambda = 2$ ,  $\nu = \eta = 10^{-11}$ . We performed  $10^7$  variable timesteps (determined by a CFL condition) with a 3<sup>rd</sup>-order Runge-Kutta numerical scheme. The time series  $\langle 2 \rangle$ , also shown on Fig. 2, was obtained with the same parameters, except that the dissipation coefficients  $\nu$  and  $\eta$  were ten times higher than for  $\langle 1 \rangle$ .

### 3.2. Coupled shell-models

Section 5 uses also data from a version of a shell-model designed to model a region of space where a dominant magnetic field  $\mathbf{B}_0$  exists, like in a coronal loop (Buchlin *et al.*, 2004). In this model, shell-models of 2D MHD are coupled by Alfvén waves travelling along  $\mathbf{B}_0$ , and energy is only input by movements of the photospheric footpoints of the loop. This geometric setup is the same as the one used for the cellular automaton described by Buchlin *et al.* (2003), and it gives a model similar to the one described by Nigro *et al.* (2004). Here we use an independent implementation of these ideas to obtain the time series  $\langle 3 \rangle$ .

### 3.3. Characteristics and intermittency of the time series

All these time series were rescaled so that their average  $\bar{\epsilon}$  is 1 and are shown on Fig 2. Their basic characteristics are summarized in table 1. From time series  $\langle 1 \rangle$  to  $\langle 3 \rangle$ , the ratio of the

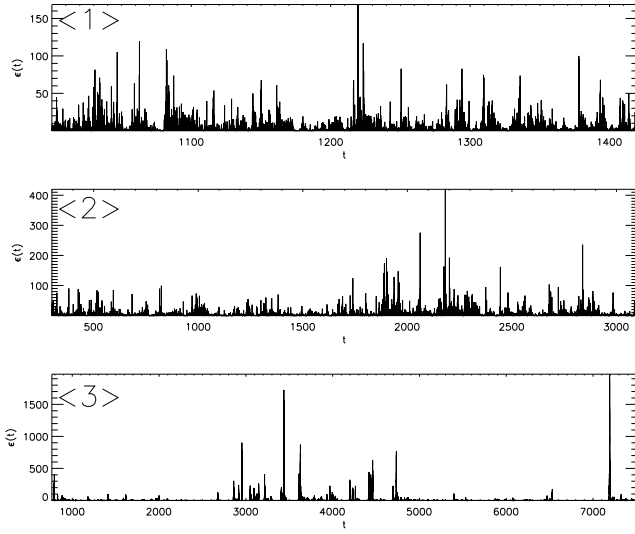


Figure 2: From top to bottom, time series  $<1>$ ,  $<2>$ , and  $<3>$ .

Table 1: Summary of the characteristics of all 3 time series, which were normalized so that their average is  $\bar{\epsilon} = 1$ : number of data points, number of peaks, standard deviation, and maximum value.

	Data points	Peaks	$\sigma_\epsilon$	$\epsilon_{\max}$
$<1>$	453,628	51,507	1.98	169
$<2>$	985,162	56,136	2.45	420
$<3>$	1,000,000	305,738	11.33	1971

maximum (or the standard deviation) to the average grows, and longer, quiet times exist between the intervals with higher dissipation. It seems that intermittency is higher for  $<3>$  than for  $<2>$ , and that it is also higher for  $<2>$  than for  $<1>$ . This is verified by plotting the flatness<sup>1</sup> of these time series as a function of the temporal scale (Fig. 3).

#### 4. Comparison between statistics for different event definitions

In this section, starting from the time series  $\epsilon(t)$  number  $<1>$  produced as explained in section 3.1, we compare the effect of the definition of an event for the following statistics:

- normalized histograms (*i.e.* experimental Probability Distribution Functions – or PDFs) of event peak dissipation power, total energy and duration, as defined by the different event definitions we use,
- PDFs of waiting times between events, *i.e.* the time between two successive events. This corresponds to the laminar, quiet time between events.

<sup>1</sup> We use the following definition for the flatness  $F(\tau)$  of the time series  $\epsilon(t)$ :  $F(\tau) = S^4(\tau)/(S^2(\tau))^2$ , where  $S^q(\tau) = \langle |\epsilon(t+\tau) - \epsilon(t)|^q \rangle_t$  is the structure function of index  $q$  for the timeseries  $\epsilon$ .

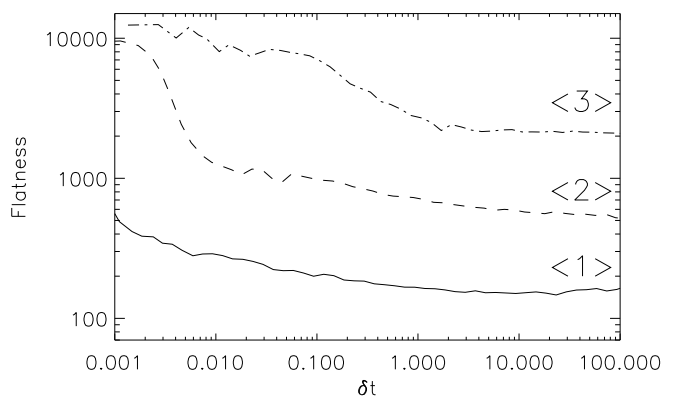


Figure 3: The flatness of the three time series increases when the scale  $\delta t$  decreases. This behavior is a signature of intermittency, and is stronger for the time series  $<3>$  and lower for time series  $<1>$ . Note that the flatness remains much higher than the Gaussian value 3 even at large time scales, as a consequence of the non-Gaussian distribution function of the values taken by the time series.

#### 4.1. Peaks

As each peak of the time series is counted as an event, definitions 1 and 1.1 give a lot of events, even in the case of our numerical data, which has no noise: for time series  $<1>$  for example, one data point over nine is a local maximum, and corresponds thus to an event. When noise is present, a smoothening of the data at the scale of the shortest events may be necessary before searching for events. Furthermore, the set of the events is a partition of the time series (the end  $t_b$  of one event is the beginning  $t_a$  of the next event), all the energy of the time series is contained in the events:  $\sum_i E_i = \int \epsilon(t) dt$ .

The distributions of  $P$ ,  $E$ ,  $T$  and  $\tau_w$  (Fig. 4) have approximately the same shape, which is neither a power-law, nor an exponential or gaussian. The tail of the waiting-time distribution could even be fitted to an exponential (Fig. 5), in contradiction with previous studies of shell-models, which used another definition of an event (Boffetta *et al.*, 1999; Lepreti *et al.*, 2001).

With these definitions, even the smallest peaks are counted as events, and this breaks the waiting times into small parts, leading to a cut-off of the tail of the waiting-time distribution. To decrease this effect, we may exclude the smallest events (*e.g.* those with a peak power lower than a given threshold) from the analysis, which gives the following variant of definition 1:

**Variant 1.2 (peak-threshold).** A threshold  $\epsilon_{\text{thr}}$  is chosen. An event corresponds to a local maximum  $\epsilon(t_m)$  in the signal  $\epsilon(t)$ , provided that  $\epsilon(t_m) > \epsilon_{\text{thr}}$ . The time of the event is  $t_e = t_m$ , the peak dissipation power is  $P = \epsilon(t_e)$ , the total dissipated energy is  $E = \int_{t_a}^{t_b} \epsilon(t) dt$  where  $t_a$  and  $t_b$  are the two local minima around  $t_e$ , and the event duration is  $T = t_b - t_a$ .

Note that this is *not* the same as using definition 2: for a given threshold  $\epsilon_{\text{thr}}$ , on a maximum connex part  $V$  of  $\{t \mid \epsilon(t) > \epsilon_{\text{thr}}\}$ , definition 1.2 will find as many events as there are peaks

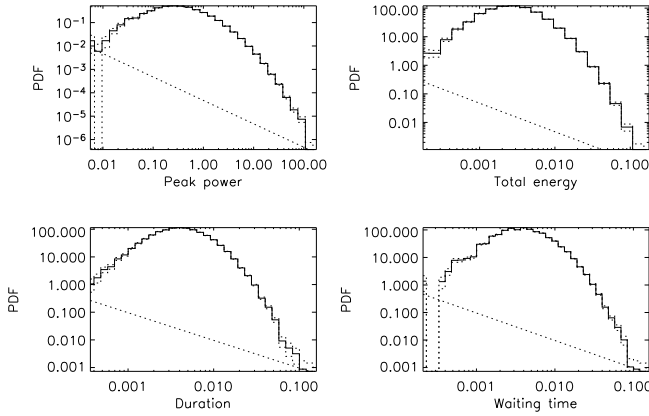


Figure 4: Events statistics of time series  $<1>$  for definition 1 (peaks): peak power of energy dissipation, dissipated energy, duration, and waiting times. The straight dashed line corresponds to one event per histogram bar; as the histogram bars are spaced exponentially, its slope is  $-1$ . The dashed histograms are an estimation of the discretization error when building the histogram, computed assuming Poisson statistics in each bar ( $\pm \sqrt{N}$  where  $N$  is the number of events in a given histogram bar).

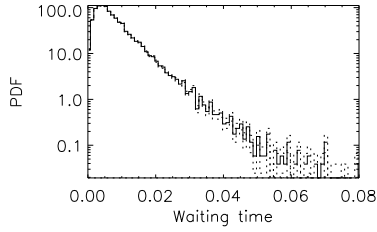


Figure 5: Waiting-time distribution of events from time series  $<1>$  for definition 1 (peaks), in lin-log scale.

of  $\epsilon(t)$  on the interval  $V$ , whereas definition 2 will find only one event.

As a result (Fig. 6), it is clear that the PDF of  $P$  is cut below the value of  $\epsilon_{\text{thr}}$ , with no modification of its shape: this means that only the tail  $P > \epsilon_{\text{thr}} = 1$  of the histogram of  $P$  in Fig. 4 is left, and this tail could be fitted to a quite narrow power-law of slope  $-2.95$ . The PDFs of  $E$  and  $D$  do not change dramatically, except that the left part is weaker because of the correlations between  $P$ ,  $E$  and  $D$ . The most interesting effect of using variant 1.2 instead of definition 1 is for the waiting-time distribution: it exhibits now a clear power-law of index  $-1.98$  over 2.5 decades. This is made possible by the fact that small waiting times associated to small events in the case of definition 1 are now replaced by a smaller number of long waiting times, leading to a reinforcement of the right part of the histogram of  $\tau_w$ .

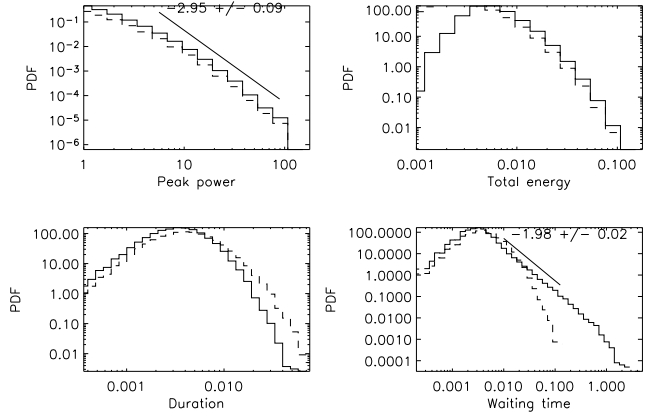


Figure 6: Events statistics of time series  $<1>$  for definition 1.2 (peak-threshold) with  $\epsilon_{\text{thr}} = 1$  (average of time series). The statistics for definition 1 (peaks) are shown as a reference, in dashed lines.

#### 4.2. Threshold

With definition 2, histograms of  $P$ ,  $E$ ,  $T$ , and  $\tau_w$  are quite clearly power-laws (Fig. 7), even if they are not very wide for this weakly intermittent time series. The slopes of these power-laws are  $2.89 \pm 0.06$  for  $P$ ,  $2.31 \pm 0.05$  for  $E$ ,  $2.48 \pm 0.06$  for  $T$ , and  $1.79 \pm 0.02$  for  $\tau_w$ .

These power-law tails still exist when the threshold is considered as a background and is removed (variant 2.1, Fig. 8), but the left part of the histograms is then almost flat in logarithmic axes. This is for example quite straight-forward for the distribution of  $P$ , as removing the background is shifting — in linear axes — the distribution of  $P$  to the left. However, the right tail of the distributions, *e.g.* for  $P \gg \epsilon_{\text{thr}}$  remains almost the same when the background is removed. It seems that background removal does not help understand the statistics of events.

Methods using a threshold are very widely used when events are searched in time series, as well from numerical simulations: Dmitruk *et al.* (1998); Einaudi *et al.* (1996); Georgoulis *et al.* (1998) (2D RMHD), Boffetta *et al.* (1999) (MHD shell-models) as from X-rays observations: Pearce *et al.* (1993); Crosby *et al.* (1993); Wheatland *et al.* (1998). It actually seems to be well-adapted to instrumental constraints of sensitivity and noise levels.

The drawbacks of this definition are that it misses the lowest-energy events (leading to a cut-off of the left part of the energy histograms), and that it cannot separate close high-energy events. This definition is also not adapted to non-stationary time series: in this case, the threshold should adapt to the local statistical characteristics of the time series.

#### 4.3. Wavelet analysis

Definition 3 produces the histograms of  $P$ ,  $E$ ,  $D$ , and  $\tau_w$  shown on Fig. 9. The histogram of events durations is a power-law over more than 2.5 decades. The wide and flat left part of the histograms of  $P$  and  $E$ , which include events much smaller than

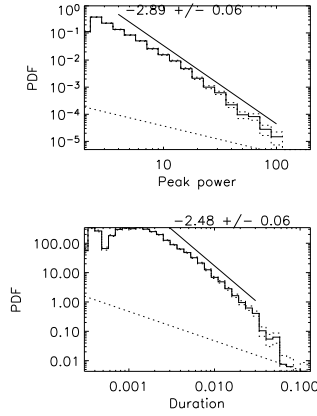


Figure 7: Events statistics of time series  $<1>$  for definition 2 (threshold).

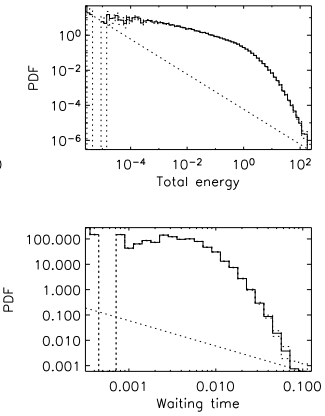
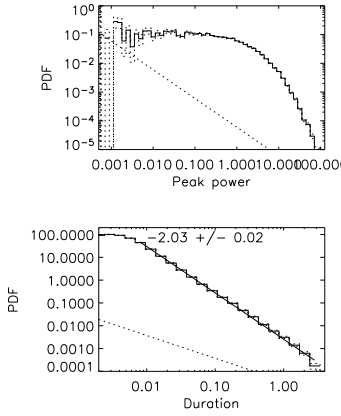
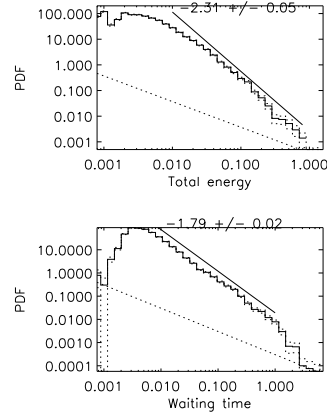


Figure 7: Events statistics of time series  $<1>$  for definition 2 (threshold).

Figure 9: Events statistics of time series  $<1>$  for definition 3 (maxima in wavelet time-scale space).

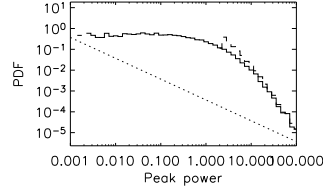
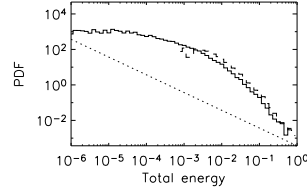


Figure 8: Events statistics of time series  $<1>$  for definition 2.1 (threshold-background). Only the distributions which are different from the one obtained by definition 2 (threshold, Fig. 7) are represented.



with other definitions, suggest to use a variant of definition 3 similar to variant 1.2 of definition 1, where the smallest events are simply not taken into account:

**Variant 3.1 (wavelet-threshold).** A threshold  $E_{\text{thr}}$  is chosen. An event corresponds to a local maximum  $y(t_e, s_e)$  in the time-scale plane  $y(t_0, s)$ , provided that  $y(t_e, s_e) > E_{\text{thr}}$ . The time of the event is  $t_e$ , its duration  $T$  is the scale  $s_e$ , its total energy is  $E = y(t_e, s_e)$ . Its peak power  $P$  can be defined as  $\max_V \epsilon(t)$  with  $V = [t_e - s_e/2, t_e + s_e/2]$ .

As for definition 1.2 (peak-threshold), the distributions of  $P$ ,  $E$  and  $D$  do not change much, but a power-law is recovered (Fig. 10) for the waiting-time distribution.

## 5. Intermittency and sensitivity to event definition

### 5.1. Sensitivity to event definition

Now we use all the 3 time series described in section 3. It seems that the distributions of event energies  $E$  obtained by definitions 1 and 3 are closer from the power-law obtained by definition 2 in the case of time series  $<3>$  (Fig. 11c) than in the case of time series  $<1>$  (Fig. 11a). The waiting-times distributions (Fig. 12) display the same behavior. In general, distributions obtained from higher-intermittency time series seem to be less sensitive to the definition of an event than low-intermittency time series.

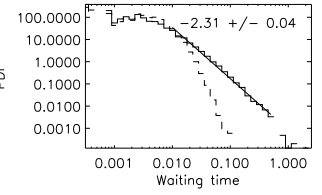
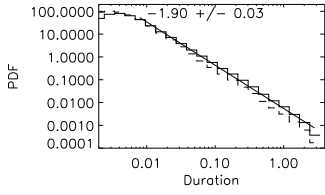
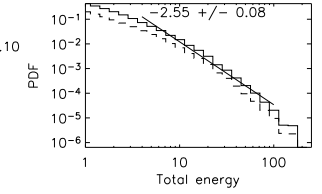
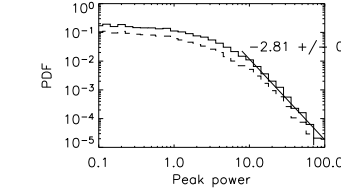


Figure 10: Events statistics of time series  $<1>$  for definition 3.1 (wavelet-threshold) and  $E_{\text{thr}} = 1$ . The statistics for definition 3 (maxima in wavelet time-scale space) are shown as a reference, in dashed lines.

### 5.2. Sensitivity to threshold, for definition 2 (threshold)

In the case of events defined by a threshold (like definition 2), the slope of event energy histograms may depend on the threshold. Here we choose different values of  $\epsilon_{\text{thr}}$  between 0 and  $\bar{\epsilon} + 5\sigma_{\epsilon}$  where  $\bar{\epsilon}$  is the time series average ( $\bar{\epsilon} = 1$ ) and  $\sigma_{\epsilon}$  is the standard deviation shown in table 1 for each of the time series. As a result, the number of events (Fig. 13e) is 1 when the threshold is  $\epsilon_{\text{thr}} = 0$  (the whole time series is *one* event); it increases to a maximum, attained between  $\bar{\epsilon}$  and  $\bar{\epsilon} + \sigma_{\epsilon}$ , depending on the time series characteristics; then it decreases (ultimately, the number of events is 0 when  $\epsilon_{\text{thr}} > \epsilon_{\text{max}}$ , where  $\epsilon_{\text{max}}$  is the maximum value of the time series).

Figure 13 shows the power-law slope of the histograms of  $P$ ,  $E$ ,  $T$ , and  $\tau_w$  as a function of the normalized threshold  $(\epsilon_{\text{thr}} - \bar{\epsilon})/\sigma_{\epsilon}$ . In general, time series  $<1>$  and  $<2>$ , which come from the same simple shell-model and which are less intermittent than the time series  $<3>$ , follow quite the same path. (a) The distributions of peak dissipation power  $P$  have a slope  $\approx 2$  for a low threshold  $\epsilon_{\text{thr}}$ , and become steeper when  $\epsilon_{\text{thr}}$  increases.

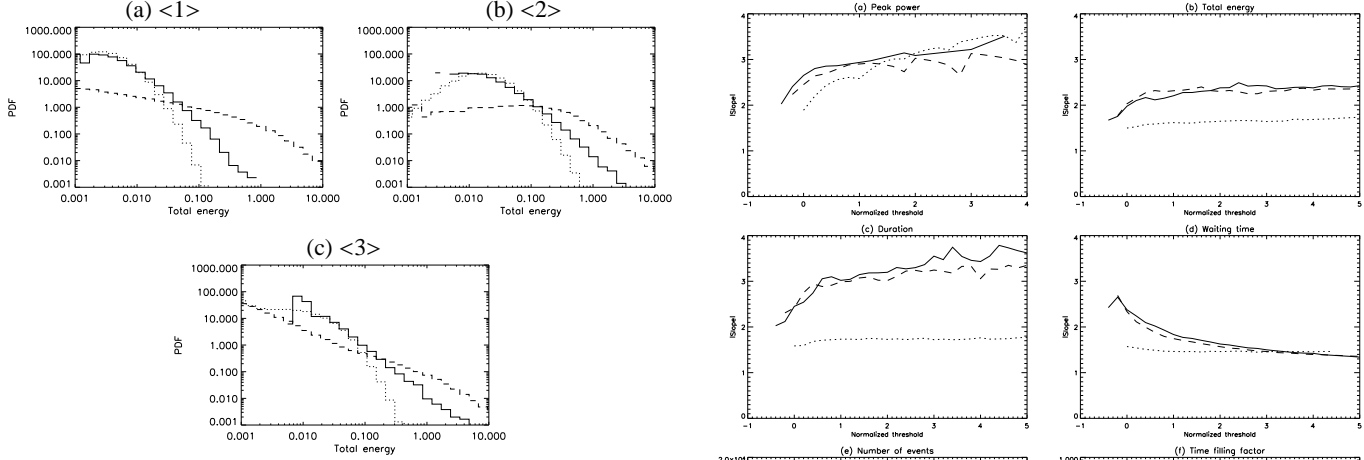


Figure 11: (a) Total energy distributions for events determined by definitions 1 (peaks; dotted line), 2 (threshold; plain line), and 3 (maxima in wavelet time-scale space; dashed line), for time series  $<1>$ . (b) Same figure for time series  $<2>$ . (c) Same figure for time series  $<3>$ . All plots have the same scale.

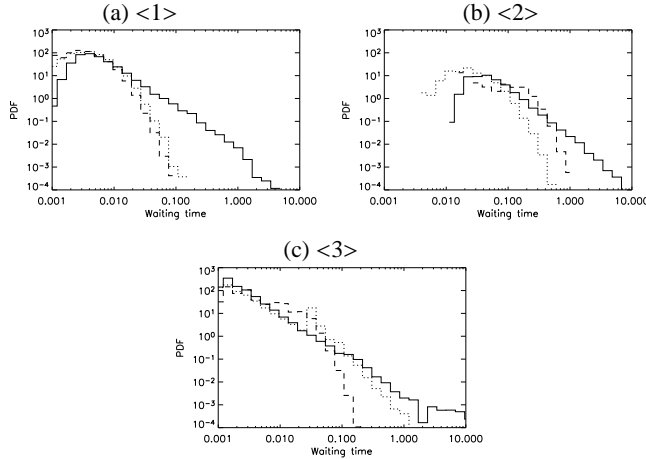


Figure 12: (a) Waiting-time distributions for events determined by definitions 1 (peaks; dotted line), 2 (threshold; plain line), and 3 (maxima in wavelet time-scale space; dashed line), for time series  $<1>$ . (b) Same figure for time series  $<2>$ . (c) Same figure for time series  $<3>$ . All plots have the same scale.

The slope for time series  $<3>$  is slightly more sensitive to  $\epsilon_{\text{thr}}$  than the other time series. (b) The slope of the distributions of energy  $E$  also increase with  $\epsilon_{\text{thr}}$ , except for time series  $<3>$ , for which it is almost constant. (c) The statistics of the durations  $T$  exhibit the same features than the statistics of  $E$ . (d) On the contrary, the slope of the distributions of the waiting times  $\tau_w$  decreases when  $\epsilon_{\text{thr}}$  increases. Again, it is almost constant for time series  $<3>$ . (f) The proportion of the time series duration contained in events decreases when the threshold increases. This decrease is stronger for the lowly intermittent time series.

Time series  $<3>$  seems to be the least sensitive to the value of  $\epsilon_{\text{thr}}$ . Note that, by using thresholds expressed as a function of  $\sigma_\epsilon$  instead of absolute thresholds, we have taken care of the

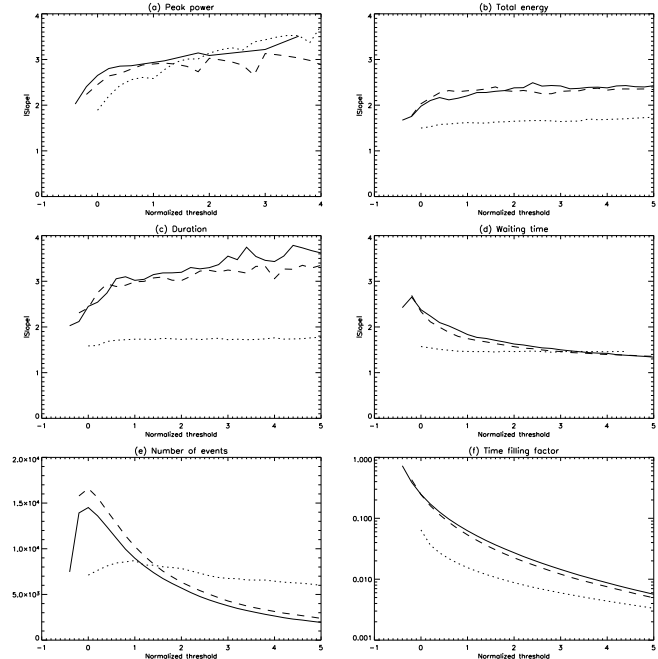


Figure 13: Slope of the peak power (a), total energy (b), duration (c), and waiting time (d) distributions, for events defined by definition 2 (threshold), as a function of the normalized threshold  $(\epsilon_{\text{thr}} - \bar{\epsilon})/\sigma_\epsilon$ . The plain, dashed, and dotted lines correspond to time series  $<1>$ ,  $<2>$ , and  $<3>$  respectively. (e) Number of events detected as a function of the normalized threshold. (f) Proportion of the duration contained in events, as a function of the normalized threshold.

fact that the deviations of time series  $<3>$  are larger than for the other time series.

## 6. Discussion

We have investigated the dependence on the definition of “events” of the statistics of events obtained from an energy dissipation time series. Not very surprisingly, the statistics of peak power, energy content, duration and waiting times of events differ when different definitions are used.

Especially for low-intermittency time series and for waiting-time distributions, power-law distributions are recovered only when a threshold is used, either when searching for events (definition 2) or after having searched for events by another means (definitions 1.2 and 3.1). It is also interesting to note that the waiting-time distribution, which is used to test the Poissonian nature of the flaring process (Wheatland *et al.*, 1998; Lepreli *et al.*, 2001; Wheatland and Litvinenko, 2002), can have a power-law or an exponential tail, depending on the definition of events.

For observational studies, where the smallest events are averaged over the line of sight and the spatial and temporal steps, some of the intermittency is lost. In this case we need to use a definition which gives statistics as close as possible from the statistics of the underlying (non-averaged) signal (which is intermittent enough for events statistics to be almost independent from their definition). The definitions using a threshold

seem to be adequate from this point of view. The presence of noise in observations gives also a strong support to this kind of definitions. However, these definitions have also drawbacks, in particular the difficulty of choosing a threshold for a non-stationary time series.

Other definitions like 3 which uses wavelets can have interesting properties separating simultaneous events at different scales, but the smallest events obtained by this means seem to be not significant. Alternatively, events could be defined iteratively from the time-scale plane: the first event is defined by the overall maximum of the time-scale plane, the corresponding wavelet is subtracted from  $\epsilon(t)$ , a new time-scale plane is computed, and this process is done again to find each of the next events. Local Intermittency Measure (LIM: Farge, 1990) could perhaps also be used for this purpose. However, these ideas have not been investigated further yet and an iterative definition may be computationally very expensive compared to the other definitions.

Let us now return to the motivation behind the determination and discussion of event properties and statistics for coronal physics. There are two main reasons for these studies, essentially related to bridging the gap between observable time and spatial scales and the sub-resolution physics. On the one hand, we would like to understand whether analogous physical processes, namely flares, conserve scale-invariant properties at unobservable scales and are responsible for the existence of the quiet corona as we know it. On the other, one would like to link, as far as possible, large scale physical models and numerical simulations to the observations without reproducing in detail the microcosm of a single small-scale event (though this may be desirable and necessary for the largest scale manifestations, such as for example the Bastille day flare), but by comparing global statistical properties.

When searching for the answer to the first question, one must clearly use an event definition which conserves the total energy in the signal, as one is searching for a quantitative confirmation (again, much care is needed, since the average corona exists to some extent precisely because we are incapable of observing fluctuations at sufficiently small energy and time-scale, *i.e.* it is by definition a background). In the second case however, where there are undoubtedly large differences between numerical models and observations in the richness of the physics and dynamical range, one must be careful to analyze events in the way most appropriate to glean characteristic properties of the fluctuations and turbulence at the available scales. Hence the requirements are to go beyond simply the energy distributions of events and analyze other characteristic features such as anisotropy of the spectra, intermittency, and higher order structure functions of the fields.

**Acknowledgements.** The authors acknowledge partial financial support from the PNST (Programme National Soleil-Terre) program of INSU (CNRS) and from European Union grant HPRN-CT-2001-00310 (TOSTISP network). E. Buchlin thanks the French-Italian University for travel support. The authors thank Jean-Claude Vial, Loukas Vlahos and Jean-François Hochedez for useful discussions.

## References

Aschwanden, M. J. and Charbonneau, P. (2002). Effects of Temperature Bias on Nanoflare Statistics. *ApJ*, **566**, L59–L62.

Aschwanden, M. J., Tarbell, T. D., Nightingale, R. W., Schrijver, C. J., Title, A., Kankelborg, C. C., Martens, P., and Warren, H. P. (2000). Time variability of the “quiet” Sun observed with TRACE. II. physical parameters, temperature evolution, and energetics of extreme-ultraviolet nanoflares. *ApJ*, **535**, 1047–1065.

Bak, P., Tang, C., and Wiesenfeld, K. (1988). Self-organized criticality. *Phys. Rev. A*, **38**, 364–374.

Biskamp, D. (1994). Cascade models for magnetohydrodynamic turbulence. *Phys. Rev. E*, **50**, 2702–2711.

Boffetta, G., Carbone, V., Giuliani, P., Veltre, P., and Vulpiani, A. (1999). Power Laws in Solar Flares: Self-Organized Criticality or Turbulence? *Physical Review Letters*, **83**, 4662–4665.

Boffetta, G., de Lillo, F., and Musacchio, S. (2002). Lagrangian statistics and temporal intermittency in a shell model of turbulence. *Phys. Rev. E*, **66**(6), 066307.

Buchlin, E., Aletti, V., Galtier, S., Velli, M., Einaudi, G., and Vial, J.-C. (2003). A simplified numerical model of coronal energy dissipation based on reduced MHD. *Astron. Astrophys.*, **406**, 1061–1070.

Buchlin, E., Velli, M., and Galtier, S. (2004). Simplified simulations of MHD in a coronal loop by coupled shell-models. In *Proceedings of the Conference SOHO 15 ‘Coronal Heating’ ESA SP*, *in press*.

Crosby, N. B., Aschwanden, M. J., and Dennis, B. R. (1993). Frequency distributions and correlations of solar X-ray flare parameters. *Sol. Phys.*, **143**, 275–299.

Dmitruk, P., Gómez, D. O., and DeLuca, E. E. (1998). Magnetohydrodynamic turbulence of coronal active regions and the distribution of nanoflares. *ApJ*, **505**, 974–983.

Einaudi, G., Velli, M., Politano, H., and Pouquet, A. (1996). Energy Release in a Turbulent Corona. *ApJ*, **457**, L113.

Farge, M. (1990). In H. Moffat, editor, *Topological Fluid Dynamics*. Cambridge University Press.

Frick, P. and Sokoloff, D. (1998). Cascade and dynamo action in a shell model of magnetohydrodynamic turbulence. *Phys. Rev. E*, **57**, 4155–4164.

Georgoulis, M. K., Velli, M., and Einaudi, G. (1998). Statistical properties of magnetic activity in the solar corona. *ApJ*, **497**, 957–966.

Giuliani, P. and Carbone, V. (1998). A note on shell models for MHD turbulence. *Europhys. Lett.*, **43**, 527–532.

Gledzer, E. B. (1973). *Sov. Phys. Dokl.*, **18**, 216.

Gloaguen, C., Léorat, J., Pouquet, A., and Grappin, R. (1985). A scalar model for MHD turbulence. *Physica D*, **17**, 154–182.

Hudson, H. S. (1991). Solar flares, microflares, nanoflares, and coronal heating. *Sol. Phys.*, **133**, 357–369.

Lepreti, F., Carbone, V., and Veltre, P. (2001). Solar Flare Waiting Time Distribution: Varying-Rate Poisson or Lévy Function? *ApJ*, **555**, L133–L136.

Lu, E. T. and Hamilton, R. J. (1991). Avalanches and the distribution of solar flares. *ApJ*, **380**, L89–L92.

Nigro, G., Malara, F., Carbone, V., and Veltri, P. (2004). Nanoflares and MHD Turbulence in Coronal Loops: A Hybrid Shell Model. *Phys. Rev. Lett.*, **92**(19), 194501.

Pearce, G., Rowe, A. K., and Yeung, J. (1993). A statistical analysis of hard X-Ray solar flares. *Astron. Astrophys. Suppl. Ser.*, **208**, 99–111.

Sanz, J. L., Herranz, D., and Martínez-Gónzalez, E. (2001). Optimal Detection of Sources on a Homogeneous and Isotropic Background. *ApJ*, **552**, 484–492.

Wheatland, M. S. and Litvinenko, Y. E. (2002). Understanding Solar Flare Waiting-Time Distributions. *Sol. Phys.*, **211**, 255–274.

Wheatland, M. S., Sturrock, P. A., and McTiernan, J. M. (1998). The Waiting-Time Distribution of Solar Flare Hard X-Ray Bursts. *ApJ*, **509**, 448–455.

Yamada, M. and Ohkitani, K. (1987). *J. Phys. Soc. Jpn.*, **56**, 4210.

Yamada, M. and Ohkitani, K. (1988a). *Progr. Theo. Phys.*, **79**, 1265.

Yamada, M. and Ohkitani, K. (1988b). *Phys. Rev. Lett.*, **60**, 983.